Chapter 9
Development of a Stability Prediction Tool for the Identification of Stable Milling Processes

D. Hömberg, E. Uhlmann, O. Rott, and P. Rasper

Abstract. This chapter deals with a new mathematical model to characterize the interaction between machine and workpiece in a milling process. The model consists of a multi-body system representing the milling machine and a linear thermo-elastic workpiece model. An extensive experimental analysis supported the development of the governing model equations. A numerical solution strategy is outlined and complemented by simulations of stable and unstable milling processes including workpiece effects. The last part covers the development of a new algorithm for the stability analysis of large milling systems.

9.1 Introduction

The interaction of process and structure is the main reason for the unwanted chatter phenomena in milling. Hence, the determination of stable cutting conditions for given structures and the design of more efficient milling machines are important research fields in production technology. Since the mathematical description of model components like machine, workpiece and process is well understood by now, the main challenge is to integrate them into a coupled model and to simulate the resulting system with tailored numerical algorithms to reproduce the stability limits and the dynamical characteristics of the real system correctly.

Accordingly, the goal of the present project was the development of a coupled model to study the dynamics of milling processes by means of time domain simulations. To cope with a necessarily long simulation time the machine structure is treated as a multi-body system and the workpiece as a thermo-elastic body. Comprehensive experimental studies performed in close cooperation between engineers and mathematicians provided the basis for the mathematical modeling, the identification of model parameters and the validation of the numerical results.

The main achievements of the present work are the consistent mathematical modeling of a complex milling system including the mathematical analysis of the derived equations [10], the numerical implementation of a time-domain simulation system

B. Denkena and F. Hollmann (Eds.): Process Machine Interactions, LNPE, pp. 203–224.
springerlink.com

and its experimental validation, experimental studies, which have revealed a temperature dependency of the stability limits.

The chapter is organized as follows: In Section 9.2, we will present the different experimental studies carried out during the modeling procedure, as well as the parameter identification and for the validation of the simulation results. Section 9.3 covers the derivation of the model equations, the development of numerical algorithms and the presentation of simulation results. The last section is devoted to some concluding remarks including the discussion of perspectives and further issues.

9.2 Experimental Analysis

9.2.1 General Setup

Machining tests were performed for experimental determination of process stability behavior and cutting forces. Hence, a commonly used measurement setup for milling experiments according to [12] was implemented to measure the specific cutting forces and to analyze the process behavior.

The tests were performed on a five-axis machining center type MAP LPZ 500, which features linear drives for the linear axes. Aluminum alloy AlZnMgCu1,5 (EN AW-7075) blocks were machined for the general experiments using a one-edge end mill cutter of High-Speed Steel (HSS) with a diameter of $d = 8.0$ mm and a side rake angle of $\gamma_f = 23°$. The size of the workpieces was $150 \times 100 \times 50$ mm. The milling tool was fixed in a heat-shrinking tool holder with a HSK-A 63 mounting shank. The workpiece was mounted on a 3-component-dynamometer type Kistler 9257A. The dynamometer was connected to three charge amplifiers type Kistler 5011. For the acquisition of the data, a measuring board from National Instruments with a maximum sampling rate of 500 kHz and a resolution of 16 bit was applied. Figure 9.1 schematically displays the measurement setup.

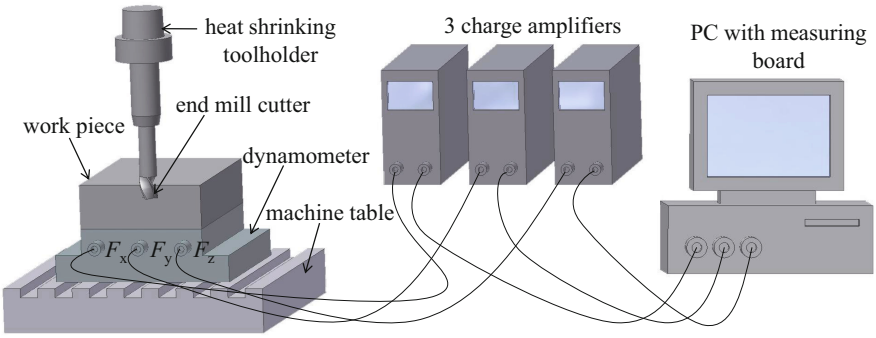

Fig. 9.1 Experimental setup for machining tests

9.2.2 Experiments for Parameter Identification

9.2.2.1 Measurement of Structural Dynamics

The identification of unknown model parameters is essential for the prediction of process stability. Therefore, the measurement of the dynamic behavior of the machine tool structure is necessary. With a similar approach as Faassen et al. [12], the dynamic characteristics of the machine structure and cutting tool can be deduced from measured mobility-frequency-response functions at the tool center point (TCP). The tool was excited in x and y-direction of the machine tool coordinate system using an impact hammer (Kistler 9722A500), while the machine tool was in an idle state. The bandwidth was 5,000 Hz. The response measurement in y-direction was realized with a laser vibrometer (Polytec OFV 303). Therefore, errors due to the additional mass of an accelerometer near the TCP were avoided as stated in [11].

9.2.3 Experimental Stability Analysis

9.2.3.1 Machining Tests for the Analysis of Process Stability and Cutting Forces

The considered process in the machining tests was peripheral end milling. Flutes with full immersion of the cutter ($a_e = 8$ mm) were machined into the workpiece. During the process, the cutting force components F_x, F_y and F_z according to the machine coordinate system were measured at the workpiece using the 3-component-dynamometer. The spindle speed was varied between $n = 15,800$ rpm and $n = 19,800$ rpm. A feed rate per tooth of $f_z = 0.2$ mm was set for each spindle speed. The cutting depths were gradually increased with 0.5 mm increments starting at 0.5 mm until the cutting process became unstable. Based on the data captured during the cutting tests the process stability behavior could be analyzed by the generation of stability charts. The process data corresponding to stable machining processes was used to determine cutting coefficients according to [23]. A sample rate of 50 kHz was used for data acquisition.

9.2.3.2 Identification of Unstable Milling Processes

A method to distinguish stable and unstable process states is necessary for the analysis of the stability behavior of cutting processes. The regenerative effect is the main reason for stable cutting processes to become unstable. Varying cutting forces lead to self-excited vibrations and an additional relative shift between tool and workpiece. These displacements create a characteristic waviness on the workpiece surface. Thus, every following cut results in a chip-thickness modulation, which is amplified by the machine tool vibrations [3], [2], [28], [33]. The characterizing frequencies of these self-excited vibrations are called chatter frequencies. The dominant chatter frequencies are generally located close to the eigenfrequencies of the considered machine tool structure. Chatter leads to a worse product quality because

of additional self-excited vibrations. Therefore, it is necessary to define a stability criterion in order to identify unstable milling processes and maintain a good product quality.

The described effect makes it possible to identify process instabilities by considerating force signals in frequency domain. Other possibilities are the analysis of vibration signals near the TCP, the resulting surface roughness, the occurrence of chatter marks and noise measurements during the machining process [12]. In this research work, the recorded cutting force signals were transformed into frequency domain using Fast-Fourier-Transformation (FFT) according to [3], [13] and [19] in order to identify the dominant frequencies and related amplitudes. Figure 9.2 shows the spectrum of the force signals for a stable and and an unstable milling process. Since a one-edge end mill cutter was used the spindle speed of $n = 17200$ rpm corresponds to excitation frequencies, which are multiples of $f = 287$ Hz.

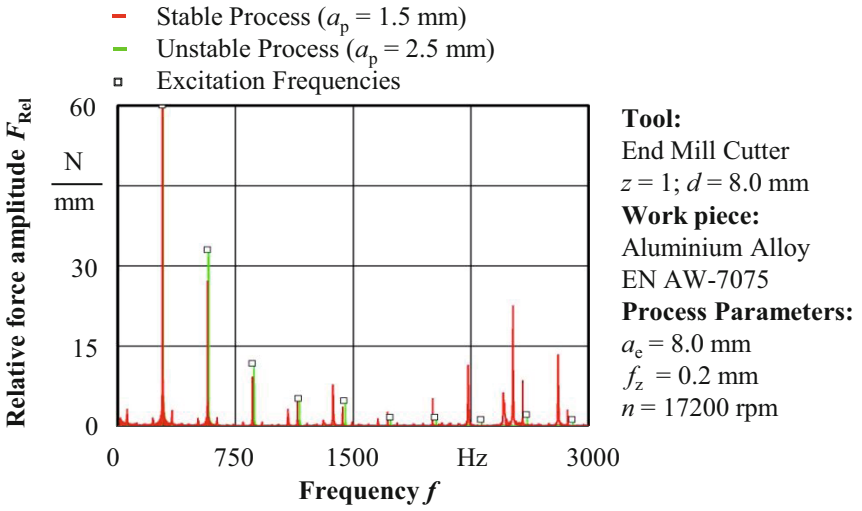

Fig. 9.2 FFT of stable and unstable cutting processes

According to Sims [27], stable and unstable process states were determined by the investigation of the ratio between the absolute value of the largest force amplitude, which can be allocated to the excitation frequency, and the largest force amplitude of the occurring chatter frequency. If the ratio exceeds a value of 10 %, the corresponding process is classified as unstable. In addition, the resulting surface roughness, the occurrence of chatter marks and noise during the machining process were also taken into account. A detailed description of the procedure is given in [29].

9.2.3.3 Results of the Stability Analysis

The measured cutting force signals were analyzed using the illustrated method for the identification of unstable cutting processes in order to generate stability plots and determine stability limits. Figure 9.3 shows the resulting stability plot.

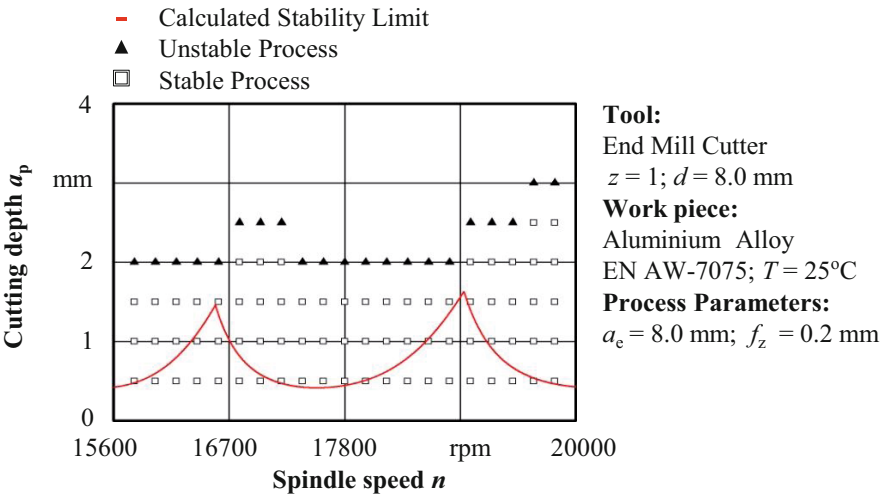

Fig. 9.3 Stability plot for a feed-rate-per-tooth of $f_z = 0.2$ mm

The variation of the stability limit is rather small in the analyzed range of spindle speed. The maximum value is $a_p = 2$ mm at spindle speeds around $n = 17,000$ rpm and $n = 19,400$ rpm. For other spindle speeds, $a_p = 1.5$ mm is the measured stability limit.

The graph depicted in Figure 9.3 has been computed using the standard stability prediction method proposed by Altintas et al. (see e.g. [2] or [1]). A mobility-frequency-response function measured by means of hammer excitation and cutting force coefficients determined from cutting force measurements under stable cutting conditions have been provided as input data.

9.2.3.4 Possible Sources of Measurement Errors in the Process Analysis

The large gap between the predicted and the measured stability limits can probably be explained with difficulties in the measurement of the frequency-response function at the tool center point. Beyond that, the dynamometer which has been mounted between machine table and workpiece, might also affect the dynamical characteristics of the structure. Both effects have been analyzed in [22]. The frequency-response function of the work piece changes significantly, if the workpiece is not directly mounted on the machine table but on the dynamometer. However, in both cases, the average value of the measured workpiece frequency-response function is about

two orders of magnitude smaller than the corresponding value at the tool center point [22]. Consequently, the effect of the dynamometer has been assumed to be negligible.

However, recent results of machining tests have shown that the dynamic behavior of the dynamometer-workpiece combination seems to have a much larger impact on process behavior as expected. Although the amplitudes of the response functions are very small, current experimental process analysis has shown that the shifting of eigenfrequencies by use of a dynamometer seems to play a major role for the stability behavior. Alternatively, the work piece accelerations during the machining tests could be monitored to detect unstable processes. By defining a new stability criterion this method would allow to remove the dynamometer and thus refine the chatter detection.

9.2.4 Workpiece Effects in Milling

9.2.4.1 Experimental Setup and Measurement Procedure

The dynamic process behavior is mainly influenced by the spindle and cutting tool of the machine tool system. Apart from that major influence, the geometry of the workpiece also has an impact on the process [5], [8]. The effect of different workpiece geometries on process stability was analyzed with an almost equal measurement setup and experimental procedure as before (see Section 9.2.1 and 9.2.2).

In this case, a more flexible T-shaped workpiece compared to the blocks with a size of $150 \times 100 \times 50$ mm in the machining tests before was analyzed. The size of the vertical bar was changed to obtain numerous and different geometries. The width of the bar was varied between $t_1 = 10$ mm and $t_2 = 20$ mm and the height between $h_1 = 50$ mm and $h_2 = 150$ mm to realize different dynamic behavior of the workpieces in terms of flexibility. The T-shaped workpiece was mounted upside down on the dynamometer so that the bar was in a vertical position. Flutes with full immersion of the same end mill cutter were milled into the T-shaped workpiece beginning at the top of the bar. Considering the stability plot above (Figure 9.3) stable process states were analyzed using different workpiece geometries.

9.2.4.2 Analysis of the Influence of the Workpiece Geometry on Process Stability

Machining test were carried out using different T-shaped workpieces. The figure points out the huge impact of the workpiece geometry on process stability behavior. With the use of the stability criterion described in Section 9.2.3.2, the considered process state was classified as stable using the aluminum block as all relevant amplitudes in the frequency domain are related to the excitation with a frequency of $f = 267$ Hz.

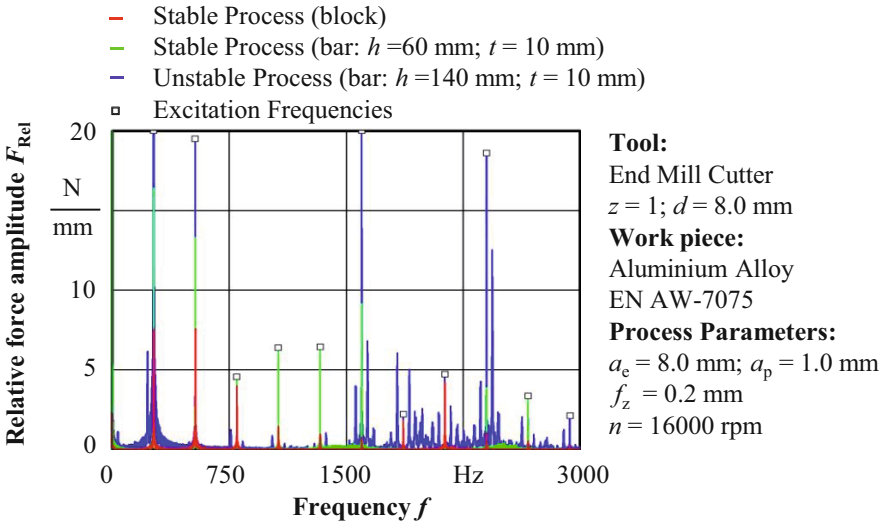

Fig. 9.4 Comparison of stability behavior considering different geometries.

The variation of the workpiece geometry leads to a varying dynamic process behavior. While the machining process remained stable for a bar with a height of $h = 60$ mm the amplitudes of the vibrations became higher in the frequency domain. When a bar with a height of $h = 140$ mm was machined the cutting process became unstable. Here, dominant chatter frequencies arise in the frequency domain apart from the excitation frequency of $f = 267$ Hz.

The results show the big impact of the workpiece geometry and thus the effect of the workpiece dynamics on process stability. It shows that there is need to consider workpiece dynamics in stability prediction. Thus, the stiffness and damping of the workpiece have to be analyzed and linked to the dynamic behavior of the machine tool structure for the calculation of stability plots.

9.2.5 Temperature Effects

9.2.5.1 Experimental Setup and Measurement Procedure

To analyze the temperature influence on process stability and cutting forces the measurement setup in Figure 9.1 was adjusted by using workpieces with different pre-heating conditions. The pre-heating of the workpiece was realized with a heating plate by Horst GmbH with three heating cartridges and a heater power of $P = 300$ W. Thus, temperatures of to $T = 200$ °C were achieved. The plate was triggered by a temperature regulator device type HT MC1.

The workpiece was warmed-up to temperatures between $T_{WP1} = 25$ °C and $T_{WP2} = 100$ °C, positioned upside down, by means of the described heating plate before the machining started. In order to ensure homogeneous heating conditions

during the machining tests thermocouples type K were fixed on the sides of the workpiece to control the local work piece temperature. In addition, the temperature was monitored using a thermal imaging camera type Infratronics IR600. Due to this approach it was possible to execute cutting tests with defined and homogeneous heating conditions ($\Delta T = 1$ K) of the workpiece.

9.2.5.2 Temperature Influence on Measurement Accuracy

The dynamometer is a piezo-electric sensor. For the analysis of thermal effects on process stability and cutting forces a possible source for measurement errors is the change in thermal conditions. In order to quantify these errors the temperature-dependency of the three-component-dynamometer and the influence on the measurement results were analyzed. The dynamometer was gradually heated to temperatures from $T_{WP1} = 25\,^{\circ}$C to $T_{WP2} = 100\,^{\circ}$C. Then, force measurements were performed using defined force signals. First, the dynamometer was loaded with defined masses in a static way; and the arising differences between the measured force signals and normal forces were determined. In a second step, an impact hammer was used excite of the dynamometer at different temperatures. The measured amplitudes and lengths of the force impulse signals by the hammer were recorded and subsequently compared with the measured signals of the dynamometer. The warming of the hammer can be neglected due to the temporally short contact between platform and impact hammer.

Only a small measurement inaccuracy of the dynamometer of about 1 % for the static case and 0.5 % for the dynamic case could be identified as a result of these approaches. Hence, a thermal decoupling between dynamometer and workpiece for the later experiments was not required. However, the variance was considered later in the analysis.

9.2.5.3 Analysis of the Influence of Temperature on Specific Cutting Forces

Linear cutting force models relate the cutting cross-section given by a_p and h to the cutting forces via an empirical constant; the so-called specific cutting force coefficients. These coefficients depend on cutting speed, workpiece material and cutter geometry (see e. g. [1], [31]). Since the workpiece material properties, i. e. especially the yield stress, and the contact conditions change with temperature, it is expected that the cutting force coefficients decrease for higher workpiece temperatures. The effect of temperature on specific cutting forces has been analyzed employing the measurement setup and experimental procedure presented in Section 9.2.1 and 9.2.2 in order to confirm this assumption. As suggested in [1], the process parameters (spindle speed $n = 16,200$ rpm, cutting depth $a_p = 1.5$ mm and feed-rate-per-tooth of $f_z = 0.2$ mm) were been chosen such that the corresponding process was stable (see Figure 9.3). The specific cutting force component K_c was calculated as shown in [1] or [17]. Figure 9.5 shows the influence of different preheating states of the workpiece between $T_{WP1} = 25\,^{\circ}$C and $T_{WP2} = 100\,^{\circ}$C on the specific cutting force coefficient K_c.

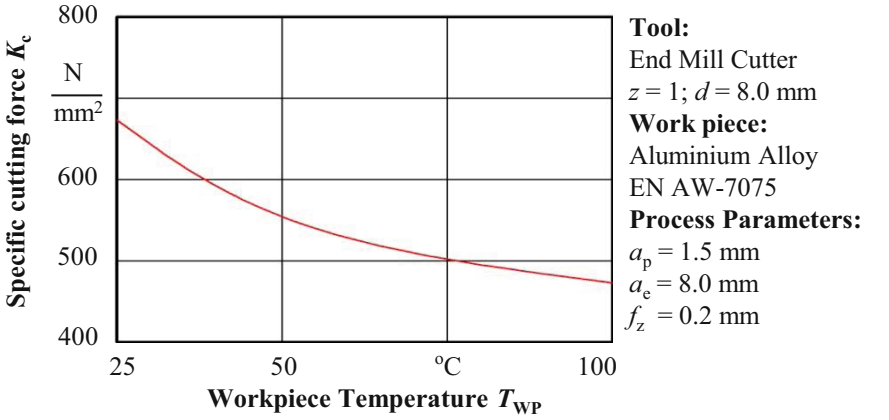

Fig. 9.5 The dependency of the specific cutting force K_c on the preheating of the workpiece

A non-linear relationship between the workpiece temperature and the specific cutting force coefficient K_c can be observed. The specific cutting force decreases with increasing workpiece temperature. The decay is about 16 % in a temperature range of $T_{WP1} = 25\,°\text{C}$ to $T_{WP2} = 50\,°\text{C}$. The decay is less important but still visible for higher workpiece temperatures. Based on these observations a new cutting force model has been developed, which incorporates the effect of the workpiece temperature on the specific cutting force. Since the diagram illustrated in Figure 9.5 exhibits an exponential decay, a similar relation was chosen for the modified specific cutting force (9.9) presented in Section 9.3.4.

9.2.5.4 Results of the Stability Analysis for Different Workpiece Temperatures

Experimental stability plots for different pre-heating conditions of the workpiece were created with use of the described measurement procedure and the illustrated method for the identification of unstable milling processes (see Figure 9.6).

Due to the pre-heating of the workpiece within the temperature range between $T_{WP1} = 25\,°\text{C}$ to $T_{WP2} = 100\,°\text{C}$, an increase of stability limits of at least $\Delta a_p = 0.5$ mm in the whole rpm-range with a maximum of $\Delta a_p = 2.0$ mm at $n = 19,400$ rpm can be determined. Only at spindle speeds between $n = 17,800$ rpm and $n = 18,400$ rpm is there no rise in the stability limits. In conclusion, higher work piece temperatures have a stabilizing effect on the process behavior.

Because of the pre-heating of the workpiece, higher temperatures occur in the cutting zone, which leads to a softening of the workpiece material so that the part of the cutting force related to plastic deformation decreases. Partially, the temperatures can reach such high levels that melting of the machined aluminum can be observed. The viscous interface between chip and tool improves the chip flow, which results in decreasing cutting forces [25], [4], [30], [14], which finally leads to increasing stability limits.

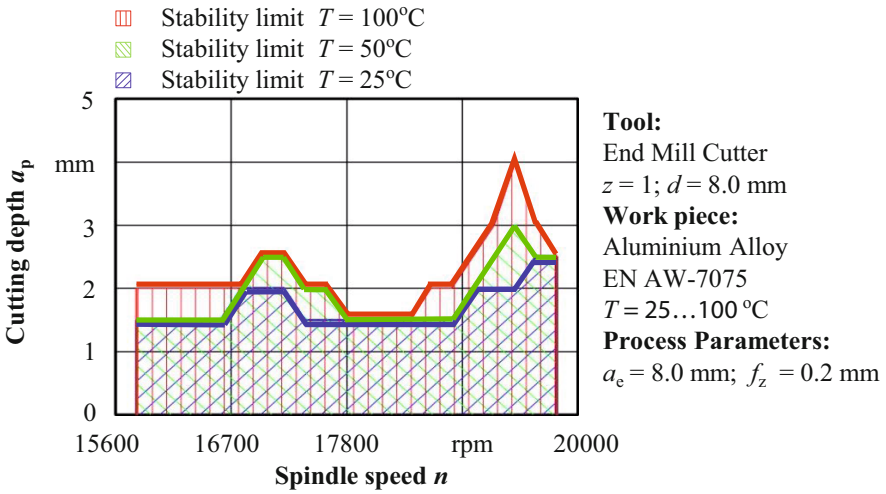

Fig. 9.6 Stability limits in dependency of the temperature

9.3 Coupled System and Simulations

9.3.1 Modeling Concept

The goal of the presented research project was the development of a complex simulation system involving the dynamical characteristics of workpiece and machine structure to study the dynamics of milling processes by means of time-domain simulations. Unstable processes can be identified by analyzing either the evolution of the uncut chip thickness or the simulated cutting force spectrum. In both cases, the precision of the predicted stability limit increases with the length of the simulated time interval. However, due to the presence of high characteristic frequencies the time-step size is strictly limited, which finally leads to unacceptable computation times, especially for models with many degrees of freedom. In view of these problems, modeling the machine structure as a multi-body system and the workpiece as a thermo-elastic work body seemed to be the best trade-off between accuracy and efficiency.

From a macroscopic point of view, the largest part of the workpiece behaves like a thermo-elastic body. Plastic deformations usually occur only in regions close to the cutting edges and can therefore be incorporated by employing an empirical cutting force model. Due to these simplifications, the material removal cannot be simulated directly and has to be approximated by a heuristic approach. For milling processes, where the difference between exit and entry angle is smaller than the pitch angle of the cutter, such an approach can be constructed by applying a method of steps. In each step the workpiece reference domain is considered to be constant and the system is solved until the cutting edge leaves the workpiece. Before the next cutting edge starts cutting, we construct a new workpiece reference domain based on the

previously computed solution and pursue the simulation. Consequently, the modeling and the simulation process consists of two parts. While the first part deals with the phenomena occurring during one tooth period, the second part focuses on the construction of a series of workpiece reference domains and thus on an implementation of the method of steps.

9.3.2 Multi-body System

The development procedure of a multi-body system representing a machine structure can be summarized as follows. The first step, an experimental modal analysis, provides the eigenfrequencies and the corresponding mode shapes. Next, considering the measured mode shapes, the rigid bodies for the model can be defined. Finally, after having implemented the mathematical model, the remaining free coupling parameters have to be identified by comparing the experimentally and numerically determined frequency-response functions for several points on the machine structure using a least-squares approach. Based on the experimental data and additional FEM simulations a multi-body system has been developed, which matches the measured frequency-response function. The final model, which is composed of cutter, tool holder, two spindle segments, headstock, x-slider and a frame moving in y-direction with respect to the fixed machine base, is illustrated in Figure 9.7.

The equation of motion describing the dynamics of the system can be summarized by the following expression

$$M(t,q)\ddot{q} = f_I(t,q,\dot{q}) + f_E(t,q,\dot{q},\eta) + g_E(t,q,F) \tag{9.1}$$

with g_E representing the external forces and torques applied via joints on each body. The parameter vector η contains the free coupling parameters, such as joint stiffness or joint damping, while M denotes the state dependent mass matrix and f_I represents the inertia forces. The last term incorporates the cutting force vector F acting on the cutter. The generalized coordinates q describe the relative motion between the rigid bodies. Due to the presence of pre-defined parameters, such as feed and spindle rotation speed the time appears explicitly in the expressions for M, f_I, f_E and g_E. Since the system is organized in a tree-like structure an iterative algorithm (c.f. [7]) can be applied to evaluate the equations of motion during a time-domain simulation.

9.3.3 Thermo-elastic Workpiece Model

The largest part of the workpiece behaves like a thermoelastic body. Plastic deformations usually occur only in regions close to the cutting edges. In the framework of a macroscopic description, the cutting forces F and the heat produced during the chip formation can be modeled by employing an empirical approach. A volume force s_E^m occurring on the right hand side represents the cutting forces acting on the workpiece. Similarly, a distributed heat source s_E^e models the heat flux into the workpiece. Note that both functions s_E^m and s_E^e depend on the cutting forces and thus

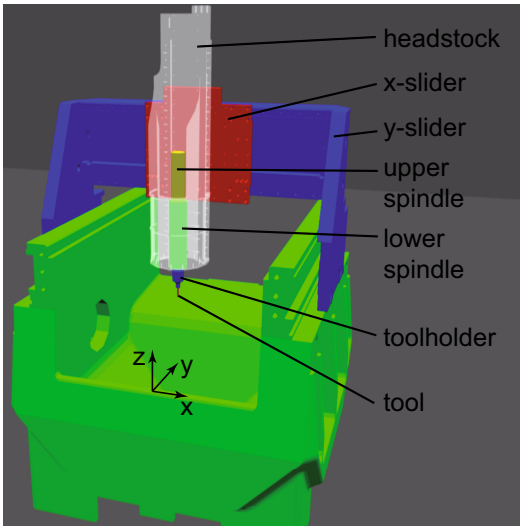

Fig. 9.7 Multi-body system representing the milling machine

on the solution of the coupled system. As shown in [15], the equations of thermo-elasticity read

$$\rho u_{tt} = \operatorname{div}(\sigma) + s_E^m, \tag{9.2}$$

$$\sigma = \lambda tr(\varepsilon) I + 2\mu\varepsilon - 3K\alpha\Theta I \quad \text{with} \quad K = (\lambda + \frac{2}{3}\mu), \tag{9.3}$$

$$\varepsilon = \frac{1}{2}\left(\nabla u + (\nabla u)^T\right), \tag{9.4}$$

$$\rho c_v \Theta_t = \kappa\Delta\Theta - 3K\alpha T_0 \operatorname{div}(u_t) + s_E^e \tag{9.5}$$

where λ and μ are the Lamé constants, ρ denotes the mass density, T_0 the reference temperature, c_v the specific heat, κ the heat conductivity and α is the thermal expansion coefficient. The function u represents the deformation field, I identity matrix and $tr(.)$ denotes the trace operator.

The heat equation has been formulated in terms of the deviation Θ from the reference temperature T_0. Thus, the actual temperature T is given by $T = \Theta + T_0$. The workpiece is fixed on a large and rigid machine table, a configuration, which can be approximated by imposing Dirichlet boundary conditions on the corresponding part of the workpiece boundary, i.e.

$$u(t,x) = 0 \quad \text{for} \quad x \in \Gamma_T, \tag{9.6}$$

$$\Theta(t,x) = 0 \quad \text{for} \quad x \in \Gamma_T. \tag{9.7}$$

9.3.4 Coupling and Material Removal Models

9.3.4.1 Coupling of Process and Structure Models during One Tooth Period

The cutting forces acting on cutter and workpiece can be described by empirical models involving the uncut chip thickness, i. e.

$$\hat{\mathbf{F}} = a_p \, \hat{\mathbf{K}}(T_{ce}) \, h, \tag{9.8}$$

where a_p denotes the depth of cut. The vector $\hat{\mathbf{K}}$ denotes an empirical parameter, the so called specific cutting force, which is usually assumed to be constant or depending on the cutting speed. However, as shown in Section 9.2.5, the cutting forces decrease due to higher workpiece temperatures. This effect has been incorporated into the cutting force model by multiplying the constant specific cutting force vector $\hat{\mathbf{K}}^{std} = [K_f, K_c, K_p]^T$ by an empirical function involving the work piece temperature T_{ce} at the cutting edge, i. e., we define

$$\hat{\mathbf{K}}(T_{ce}) = \hat{\mathbf{K}}^{std} \, (cT_{ce})^{-b}, \tag{9.9}$$

with further fit parameters b and c. The uncut chip thickness h generally depends on the current position of the cutting edge, the workpiece deformation and the shape of the workpiece surface created by the preceding tooth. In the mathematical models delay terms are often used to incorporate the effect of the surface shape (see [10]). However, to allow for a numerically stable and realistic coupling to the workpiece, an alternative approach is pursued here. The workpiece surface shall be constructed employing a real material removal model similar to the approaches presented in [9], [32].

To derive a formula for the uncut chip thickness, we assume at first that the workpiece reference configuration Ω_R is given and show how the uncut chip thickness can be derived from the current cutter position given by the solution of (9.1) and the displacement field corresponding to (9.2). Note that for presentation purposes we consider only the special case that the cutter axis is parallel to the z-axis of the workpiece reference frame. In the general case, additional transformations depending on the solution of (9.1) have to be applied to compute the vector components in the reference frame of interest.

As illustrated in Figure 9.8, a point on the cutting edge can be characterized by the vector $\mathbf{r}_{ce} = \tilde{\mathbf{r}}_{ce}(t,q,z) = \mathbf{r}_{ca} + \mathbf{r}_{ae}$. Note that the dashed lines in Figure 9.8 represent the ideal tooth path without machine and workpiece deformations. The current workpiece domain $\Omega(t)$ is given by the reference configuration Ω_R and the displacement field corresponding to (9.2), i.e. $\mathbf{x} = \mathbf{X} + \mathbf{u}(t,\mathbf{X})$ with $\mathbf{x} \in \Omega(t)$ and $\mathbf{X} \in \Omega_R$. As shown in [10], [23] and indicated by the bar labeled 'h' in Figure 9.8, the uncut chip thickness is the distance between a point 'ce' on the cutting edge and the workpiece surface measured in the direction of $\mathbf{r}_{ae}$. Mathematically, this can be formulated as follows

$$h(t,q,z,\Omega(t)) = \begin{cases} 0 & \text{if } \mathbf{r}_{ce} \notin \Omega(t), \\ \max\limits_{h^* \in \mathbb{H}} h^* & \text{otherwise,} \end{cases} \tag{9.10}$$

with the set $\mathbb{H}$ being defined as

$$\mathbb{H} = \left\{ x \in \mathbb{R}_+ \middle| \left(\mathbf{r}_{ce} - x \frac{\mathbf{r}_{ae}}{\|\mathbf{r}_{ae}\|} \right) \in \Omega(t) \right\}. \tag{9.11}$$

Combining the expression for the uncut chip thickness with the empirical cutting force model (9.8) divided by a_p gives a force per unit length, which possibly assume different values on each z-level, i.e.

$$\hat{\mathbf{R}} = \hat{\mathbf{K}}\, h(t,q,z,\Omega(t)). \tag{9.12}$$

Since the components of the vector $\hat{\mathbf{R}}$ (see Figure 9.8) are given with respect to the reference frame corresponding to the cutting edge, (9.12) has to be transformed by means of an orthogonal transformation $O(\varphi(z))$ in the cutter reference frame to compute the cutting force per unit length acting on the cutter, i. e.

$$\tilde{\mathbf{R}} = O(\varphi(z))\hat{\mathbf{R}} = O(\varphi(z))\hat{\mathbf{K}}\, h(t,q,z,\Omega(t)), \tag{9.13}$$

with $\varphi(z)$ denoting the angle between $\mathbf{r}_{ce}$ and the x-axis of the cutter reference frame. Integrating (9.13) along the cutter axis finally provides the resultant force acting on the cutter.

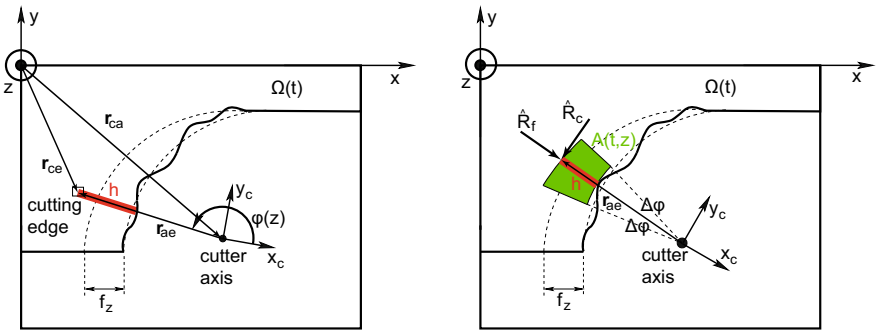

Fig. 9.8 Uncut chip thickness (left) and definition of the volume force (right)

Similar to the resulting force on the cutter, the volume forces s_E^m acting on the right hand side of (9.2) also have to be calculated from the relative cutting force given in (9.12). Applying a second orthogonal transformation $Q(t,q)$, which depends on the solution of (9.1) to (9.13) provides the components of the relative cutting force in the workpiece reference frame, i. e.

$$\mathbf{R} = Q(t,q)\tilde{\mathbf{R}} = Q(t,q)O(\varphi(z))\hat{\mathbf{K}}\, h(t,q,z,\Omega(t)). \tag{9.14}$$

Since the presented model is a macroscopic approach, which cannot reproduce the chip formation, the relative cutting forces have to be distributed over an area $A(t,z)$ located between cutting edge and workpiece surface. As illustrated in Figure 9.8, for a given point on the cutting edge $\mathbf{r}_{ae}$ and a given level z the area $A(t,z)$ is defined as the set of all points in $\Omega(t)$ enclosed by the disc-ring segment with label '$A(t,z)$'. The segment is defined by the arcs through $\mathbf{r}_{ae}$ with radius $D/2$ and length $\Delta\varphi D$ and through $(1-h/\|\mathbf{r}_{ae}\|)\mathbf{r}_{ae}$ with radius $D/2-h$ and length $2\Delta\varphi(D/2-h)$. Thus, the volume force reads

$$s_E^m(t,x,y,z) = \begin{cases} 0 & \text{if } (x,y) \notin A(t,z), \\ \frac{\mathbf{R}}{A(t,z)} & \text{otherwise.} \end{cases} \tag{9.15}$$

The heat conducted into the workpiece can be computed from the specific cutting forces and the given cutting conditions (see [26]). If the shear angle appearing in the corresponding expressions is estimated by an analytical formula as, for example, proposed in [20], the total heat flux into the workpiece denoted by $H(h,\hat{\mathbf{K}})$ can be written in explicit form. The corresponding term appearing on the right hand side of (9.5) reads

$$s_E^e(t,x,y,z) = \begin{cases} 0 & \text{if } (x,y) \notin A(t,z), \\ \frac{H(h,\hat{\mathbf{K}})}{A(t,z)} & \text{otherwise.} \end{cases} \tag{9.16}$$

9.3.4.2 Material Removal Model

As mentioned before, the workpiece surface can be constructed by employing a material removal model. The main idea is to construct a volume based on the cutting edge path and workpiece deformations, which can be subtracted from a given workpiece domain by means of Boolean operations (see e.g. [32]).

To this end, recall that during one tooth period each point on the cutting edge follows a certain path depending on the motion of the cutter. In a subinterval, some points of the cutting edge penetrate the deformed workpiece surface and the cutter is cuts. Thus, a workpiece deformation can be associated to each point $\mathbf{r}_{ce}$ of the cutting edge in the workpiece domain $\Omega(t)$, i. e.

$$\mathbf{r}_{ce} = \mathbf{X}_{ce} + \mathbf{u}(t,\mathbf{X}_{ce}), \quad \mathbf{X}_{ce} \in \Omega_R. \tag{9.17}$$

With solution $\mathbf{X}^*_{ce}(t,\mathbf{r}_{ce})$ of the above equation and the cutting edge points we define a new point $\mathbf{y}$, which corresponds either to the cutting edge or to the new shape of the reference domain, i. e.

$$\mathbf{y}(t) = \begin{cases} \mathbf{r}_{ce} & \text{if } \mathbf{r}_{ce} \notin \Omega(t), \\ \mathbf{X}^*_{ce}(t,\mathbf{r}_{ce}) & \text{otherwise.} \end{cases} \tag{9.18}$$

Monitoring these points $\mathbf{y}(t) \subset \mathbb{R}^3$ during a time interval, which encloses the actual cutting period, gives a set of points describing an open surface in the three-dimensional space. From such a surface, we construct a set $\Omega_c \subset \mathbb{R}^3$, which represents the points travelled by the cutting edge and incorporating the workpiece deformations. The new workpiece reference domain Ω_R^{new} can be found by subtracting the domain Ω_c from the given workpiece reference domain Ω_R, i.e.

$$\Omega_R^{new} = \Omega_R \setminus \Omega_c. \tag{9.19}$$

The presented strategy leads to a series of workpiece domains, each incorporating the motion of the cutting edge and the corresponding workpiece deformations during the preceding tooth path. Together with the expression for the uncut chip thickness, the model leads to a non-linear system of coupled ordinary and partial differential equations. The history of workpiece and cutter motion is stored in the workpiece surface.

9.3.5 Numerical Algorithm, Implementation and Parameter Identification

The main solution algorithm is composed of two parts. While the first part deals with the solution of the coupled system on a constant reference domain, the second part is focused towards the construction of a series of reference domains and the corresponding initial conditions.

As shown in the previous sections, the process structure interaction leads to a strong coupling of workpiece and machine model. In addition to the finite element discretization of the workpiece equations, a tailored time-integration algorithm has been developed for the coupled system guaranteeing a fully-implicit coupling of the complete system. This strategy required a large programming effort. Since standard finite element libraries do not allow the incorporation of multi-body systems, and contrarily, the standard multi-body simulation packages do not provide any tools to integrate coupled PDE-systems into the simulation environment, the numerical implementation of both parts had to be developed in the framework of an in-house library. The result is a powerful milling simulation system. Its main features are an optimal resolution of the coupling effects by an efficient implicit time-integration scheme, and as a consequence of the material removal model, the spatial resolution of the machined workpiece surface. An example for the generated workpiece surface employing a Dexel model similar to [34] is illustrated in Figure 9.9 for a stable process and in Figure 9.10 for an unstable process, respectively. In addition, the presented approach allows for the identification of machine and workpiece parameters by means of standard Gauss-Newton methods.

The identification process was carried out in close cooperation between experimenters and mathematicians. Based on the standard experiments, i. e. measurement of mobility-frequency response functions, cutting forces and temperatures, the experimental and the numerical methods have been successively adjusted in order to finally provide a realistic milling model.

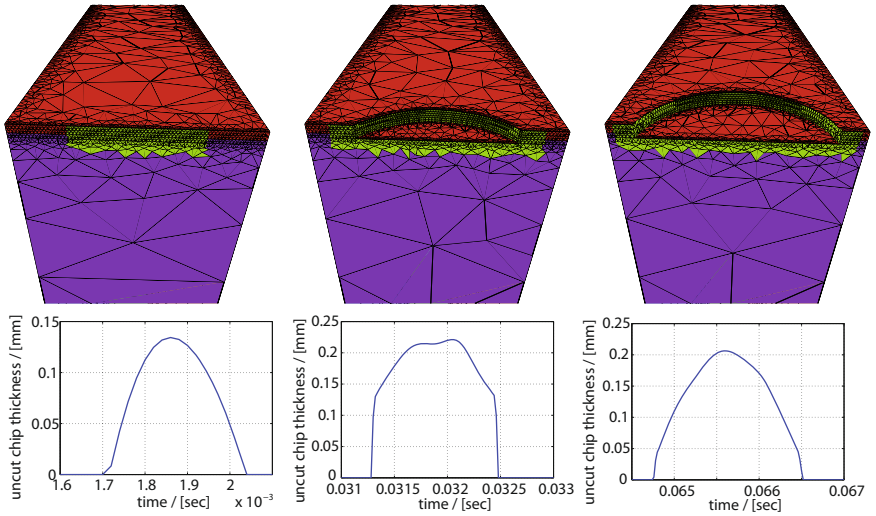

Fig. 9.9 Example for the material removal simulation, i. e. the evolution of the workpiece shape, and the corresponding uncut chip thickness in case of a stable cut

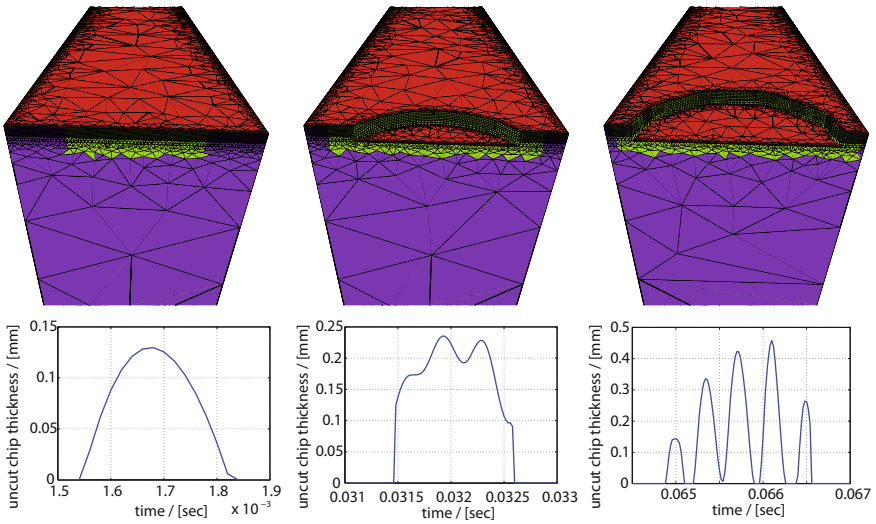

Fig. 9.10 Example for the material removal simulation, i. e. the evolution of the workpiece shape, and the corresponding uncut chip thickness in case of an unstable cut

9.3.6 Simulations

The coupled model and the developed simulation algorithm provide a tool to investigate the characteristics of milling processes involving the dynamics of machine

and workpiece. Although the temperature effects presented in Section 9.2.5 can be reproduced with the presented model, an illustration of the related phenomena is beyond the scope of this work. Therefore, we focued on effects, which can be simulated with an elastic workpiece model. Due to this restriction the workpiece equations can be reduced to system (9.2)-(9.4) with a constant temperature, i.e. $\Theta = 0$. The damping effects in the workpiece were incorporated into the model on the space discrete level, introducing a so-called Rayleigh damping term. Again, the unknown damping parameters were determined by comparing simulated and measured frequency-response functions. Recall that the vector of unknown parameters in (9.1) has been fitted so that the multi-body system reproduces the measured frequency-response functions at the tool centre point (TCP). Moreover, the cutting force model employed in [22] to compute the stability limit illustrated in Figure 9.3 is similar to (9.8). Consequently, a system composed of the machine model and a rigid workpiece almost has the same stability limits as the system analyzed to compute the red line in Figure 9.3.

As observed in the experiments, a supple workpiece structure or the wrong choice of cutting depth and spindle speed may destabilize the milling process. In order to display these effects numerically we considered three examples.

In the first simulation, the workpiece structure is rather stiff and the process parameters have been chosen so that no chatter occurs ($a_p = 0.5$ mm and $n = 16,400$ rpm, see Figure 9.3).

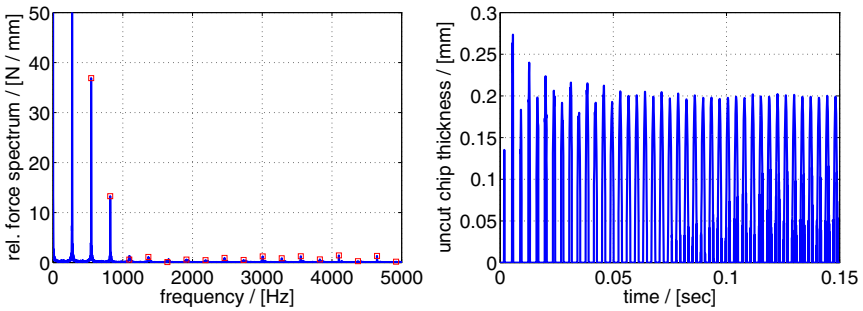

Fig. 9.11 Relative cutting force spectrum and evolution of the uncut chip thickness corresponding to a stable cut

Figure 9.11 illustrates the spectrum of the cutting force in x-direction divided by a_p and the evolution of the uncut chip thickness. Both diagrams indicate that the process is stable. No chatter peaks arise in the force spectrum and the uncut chip thickness converges to the stationary evolution.

For the second example, the spindle speed has been set to $n = 17,800$ rpm. In this case, the process parameters correspond to unstable cutting conditions. Additional chatter peaks occur in the relative force spectrum (spectrum of the cutting force in x-direction divided by a_p) depicted in Figure 9.12. According to the considerations

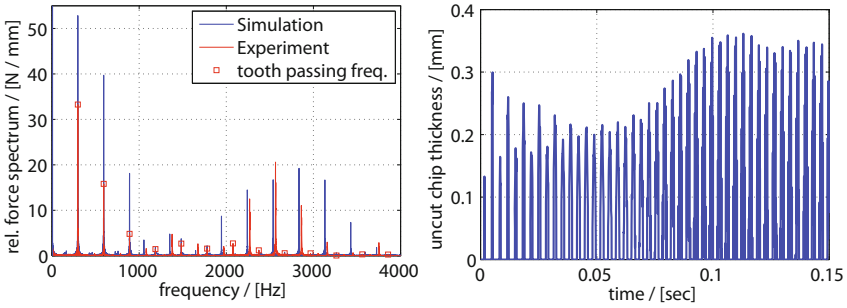

Fig. 9.12 Simulated and measured relative cutting force spectrum and evolution of the uncut chip thickness corresponding to an unstable cut

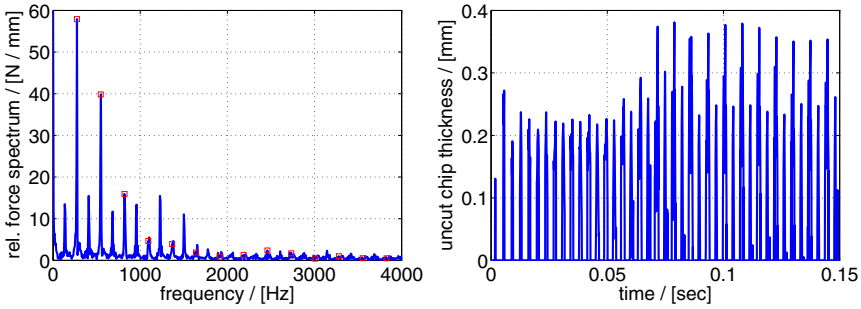

Fig. 9.13 Relative cutting force spectrum and evolution of the uncut chip thickness corresponding to an unstable cut due to a supple workpiece

outlined in Section 9.2.4.2 and 9.2.3.2 the additional chatter peaks clearly indicate that the corresponding process is unstable.

The evolution of the uncut chip thickness illustrated in Figure 9.12 confirms this result. In contrast to the evolution shown in Figure 9.11, the uncut chip thickness does not converge to the stationary evolution but increases noticeably after a short decay at the beginning and remains on a high level until the end of the simulation.

In the third example, the process parameters have been set to the same values as in the first simulation ($a_p = 0.5$ mm and $n = 16400$ rpm). The stiff workpiece utilized in the first example has been replaced by a more supple structure. Especially on top, the supple workpiece exhibits a high compliance, which can destabilize the previously stable milling process.

Analyzing the evolution of the uncut chip thickness reveals that the process does not converge to a stationary regime. Large workpiece oscillations lead to an increasing uncut chip thickness and thus to increasing cutting forces. The additional chatter peaks appearing in the relative force spectrum clearly indicate that the corresponding process is unstable. In contrast to the second example, the highest chatter peak

is not located at 2,834 Hz at but at 408 Hz. Thus, the weak spot in the structure leading to chatter vibrations is different in the two examples.

9.4 Conclusions

The goal of this chapter was the development of a complex milling model to investigate effects of machine and workpiece structure on the stability of milling processes. The experimental analysis in Section 9.2 reveals that the stability limits can be increased by pre-heating the workpiece. Moreover, it illustrates how milling processes can become unstable due to a lack of workpiece stiffness. The experiments conducted for the identification of machine parameters display that the frequency-response functions at the TCP strongly depend on the excitation method and vary with the angular spindle position. The simulations in Section 9.3 clearly demonstrate that the developed model is capable of reproducing the instability effects observed in the experiments. For the first time a new stability analysis method allows the determination of stability limits of large DDE-systems with periodic coefficients.

The results are promising and open up various directions for future research. A challenging task would be to investigate the stability of milling processes with respect to variations in the machine design.

Finally, from the application point of view, an efficient numerical tool for the systematic derivation of stability diagrams is most desirable. The developed stability analysis tool is a first step in this direction. The improvement of the numerics and the exploitation of model reduction techniques to increase the efficiency of the method will be subject to further research.

References

1. Altintas, Y.: Manufacturing Automation–Metal Cutting Mechanics, Machine Tool Vibrations, and CNC Design. Cambridge University Press (2000)
2. Altintas, Y., Budak, E.: Analytical prediction of stability lobes in milling. Ann. of the CIRP 44(1), 357–362 (1995)
3. Altintas, Y., Weck, M.: Chatter stability of metal cutting and grinding. Ann. of the CIRP 53(2), 619–642 (2004)
4. Amin, A.K.M.N., Abdelgadir, M.: The Effect of Preheating of Work Material on Chatter During End Milling of Medium Carbon Steel Performed on a Vertical Machining Center (VMC). J. of Manuf. Sci. and Eng. 125, 674–680 (2003)
5. Budak, E.: Mechanics and dynamics of milling thin walled structures. Ph.D. Thesis, University of British Columbia, Vancouver, Canada (1994)
6. Bueler, E.: Error Bounds for Approximate Eigenvalues of Periodic-Coefficient Linear Delay-Differential Equations. SIAM J. Numer. Anal. 45(6), 2510–2536 (2007)
7. Bremer, H., Pfeiffer, F.: Elastische Mehrkörpersysteme. B. G. Teubner, Stuttgart (1992)
8. Campa, F.J., López de Lacalle, L.N., Lamikiz, A., Sánchez, J.A.: Selection of cutting conditions for a stable milling of flexible parts with bull-nose end mills. J. of Mater. Proc. Technol. 191, 279–282 (2007)

9. Campomanes, M.L., Altintas, J.: An improved Time Domain Simulation for Dynamic Milling at Small Radial Immersions. Transactions of the ASME (2003), doi:10.1115/1.1580852
10. Chelminski, K., Hömberg, D., Rott, O.: On a thermomechanical milling model. Nonlinear Analysis Real World Applications 12, 615–632 (2010)
11. Ewins, D.J.: Modal Testing: Theory and Practice. Res. Stud. Press LTD. (1986)
12. Faassen, R.P.H., van de Wouw, N., Oosterling, J.A.J., Nijmeijer, H.: Prediction of regenerative chatter by modelling and analysis of high-speed milling. Int. J. of Mach. Tools & Manuf. 43, 1437–1446 (2003)
13. Faassen, R.P.H.: Chatter Prediction and Control for High-Speed Milling - Modelling and Experiments. Dissertation, TU Eindhoven, Netherlands (2007)
14. Gatto, A., Iuliano, L.: Chip Formation Analysis in High Speed Machining of a Nickel Base Superalloy with Silicon Carbide Whisker-Reinforced Alumina. Int. J. of Mach. Tools & Manuf. 34, 1147–1161 (1994)
15. Haupt, P.: Continuum Mechanics and Theory of Materials. Springer, Berlin (2000)
16. Hughes, T.J.R.: The finite element method. Dover Publications, New York (2000)
17. Insperger, T., Stépán, G.: Stability of the milling process. Period. Polytech. – Mech. Eng. 44(1), 47–57 (2000)
18. Insperger, T., Stépán, G.: Updated semi-discretization method for periodic delay-differential equations with discrete delay. Int. J. Numer. Methods Eng. 61(1), 117–141 (2004)
19. Insperger, T., Mann, B.P., Surmann, T., Stépán, G.: On the chatter frequencies of milling processes with runout. Int. J. of Mach. Tools & Manuf. 48, 1081–1089 (2008)
20. Lee, E.H., Schafer, B.W.: The Theory of plasticity applied to a problem of machining. Journal of Applied Mechanics 18, 405–413 (1951)
21. Mann, B., Insperger, T., Bayly, P.V., Stépán, G., Schmitz, T.L., Peters, D.A.: Effects of Radial Immersion and Cutting Direction on Chatter Stability in End-Milling. In: N.N. (ed.) Proceedings of the International Mechanical Engineering Conference and Exposition (IMECE), New Orleans, LA (2002)
22. Rasper, P., Rott, O., Hömberg, D., Uhlmann, E.: Analysis of uncertainties in the stability prediction for milling processes. In: Altintas, Y. (ed.) Proceedings, CIRP 2nd International Conference Process Machine Interactions (2010)
23. Rott, O., Rasper, P., Hömberg, D., Uhlmann, E.: A milling model with thermal effects including the dynamics of machine and work piece. In: Denkena, B. (ed.) Proceedings, 1st International Conference on Process Machine Interactions, PZH Produktionstechnisches Zentrum GmbH, Hannover-Garbsen (2008)
24. Rott, O., Jarlebring, E.: An iterative method for the multipliers of periodic delay-differential equations and the analysis of a PDE milling model. In: Vyhlidal, T. (ed.) Proceedings of the 9th IFAC Workshop on Time Delay Systems, Prague (2010)
25. Schulz, H.: Hochgeschwindigkeitsfräsen metallischer und nichtmetallischer Werkstoffe. Carl Hanser Verlag, München (1989)
26. Shaw, M.C.: Metal Cutting Principles. Oxford University Press, Oxford (2005)
27. Sims, N.D.: The self-excitation damping ratio: A chatter criterion for time-domain milling simulations. J. of Manuf. Sci. and Eng., Trans. of the ASME 127(3), 433–445 (2005)
28. Uhlmann, E., Mense, C.: Analysis of the Milling Machine Operation Behaviour for Process Stability and Machine Tool Optimisation. In: N.N. (ed.) Proceedings of 10th CIRP Int. Workshop on Model. of Mach. Oper., Reggio Calabria, Italy (2007)
29. Uhlmann, E., Rasper, P.: Temperaturabhängiges Stabilitätsverhalten–Untersuchung des Temperatureinflusses auf das Stabilitätsverhalten beim Umfangsstirnfräsen. In: wt Werkstattstechnik online, Düsseldorf, Germany, vol. 7(8), pp. 464–469 (2009)

30. Venuvinod, P.K., Lau, W.S., Narasimha Reddy, P., Rubenstein, C.: On the Formation of a Fluid Film at the Chip Tool Interface in Rotary Machining. Ann. of the CIRP 32, 59–64 (1982)
31. Weck, M., Teipel, K.: Dynamisches Verhalten spanender Werkzeugmaschinen. Springer, Berlin (1977)
32. Weinert, K., Surmann, T.: Geometric Simulation of the Milling Process for Free Formed Surfaces. In: Weinert, K. (ed.) Simulation Aided Offline Process Design and Optimization in Manufacturing Sculptured Surfaces, Witten (2003)
33. Zatarain, M., Munoa, J., Peigné, G., Insperger, T.: Analysis of the Influence of Mill Helix Angle on Chatter Stability. Ann. of the CIRP 55(1) (2006)
34. Zeng, W., Peng, X., Leu, M.C., Zhang, W.: A Novel Contour Generation Algorithm for Surface Reconstruction From Dexel Data. Journal of Computing and Information Science in Engineering 7, 203–210 (2007)